atmosphere

MDPI

Article

Spatial and Temporal Variation of the Extreme Saharan Dust Event over Turkey in March 2016

Hakki Baltaci

Turkish State Meteorological Service, Kütükçü Alibey Caddesi No.4, Ankara 06120, Turkey; baltacihakki@gmail.com; Tel.: +90-2164-573-400; Fax: +90-2164-573-403

Academic Editor: Robert W. Talbot
Received: 27 December 2016; Accepted: 14 February 2017; Published: 17 February 2017

Abstract: In this study, the influence of an extraordinary Saharan dust episode over Turkey on 23–24 March 2016 and the atmospheric conditions that triggered this event were evaluated in detail. PM_{10} (particulate matter less than 10 µm) observations from 97 air quality stations, METAR (Meteorological Terminal Aviation Routine Weather Report) observations at 64 airports, atmospheric soundings, and satellite products were used for the analysis. To determine the surface and upper levels of atmospheric circulation, National Centers of Environmental Prediction (NCEP)/National Center for Atmospheric Research (NCAR) Reanalysis data were applied to the extreme dust episodes. On 23 March 2016, high southwesterly winds due to the interaction between surface low- and high-pressure centers over Italy and Levant basin brought thick dust particles from Libya to Turkey. The daily PM_{10} data from 43 stations exceeded their long-term spring means over Turkey (especially at the northern and western stations). As a consequence of the longitudinal movement of the surface low from Italy to the Balkan Peninsula, and the quasi-stationary conditions of the surface high-pressure center allowed for the penetration of strong south and southwesterly winds to inner parts of the country on the following day. As a consequence, 100%, 90%, 88%, and 87% of the monitoring stations in Marmara (NW Turkey), central Anatolia, western (Aegean) and northern (Black Sea) regions of Turkey, respectively, exhibited above-normal daily PM_{10} values. In addition, while strong subsidence at the low levels of the atmosphere plays a significant role in having excessive daily PM_{10} values in Black Sea, dry atmospheric conditions and thick inversion level near the ground surface of Marmara ensured this region to have peak PM_{10} values ~00 Local Time (LT).

Keywords: Saharan dust; air quality; synoptic analysis; METAR; Turkey

1. Introduction

Dust outbreaks are considered to be one of the major natural hazards that affect the daily life. As a consequence of the intense dust storm, mineral aerosols of the desert dust are transported up to thousands of kilometers away from the source regions by atmospheric circulation. From the desert dusts, Saharan dust is known as the largest source of aeolian soil dust [1]. Previous studies showed that dust originating from the Sahara is mainly transported to the Caribbean and South America [2,3], the Mediterranean and Europe [4], the eastern Mediterranean (EM hereafter), and the Middle East [5]. Due to the transfer of the Saharan dust to distant places of the world, numerous studies investigated its impacts on health problems (e.g., [6–11]), atmospheric heating and stability [12], cloud formation and radiation [13], and visibility [14], from regional perspectives. In the EM basin (extending from Turkey to northern Africa and eastward to Iran), dust loadings originating from Sahara are shown mostly in spring months [15] due to the occurrence of intense Sharav cyclones, which are generated by the thermal contrast between cold Atlantic air and warm continental air, over the south of the Atlas Mountains (Morocco). As a consequence of these high energetic Sharav cyclones, mobilized dust is transported to eastward directions with a typical speed of 7–8 degrees of longitude (~700–800 km) per day [5]. Therefore, many researchers investigated the relationship between synoptic-scale circulation patterns and dust particles by focusing on extreme case events in this EM region. Tsidulko [16] investigated the significant variation of the dust layers within the cyclone centers using the Eta weather and dust prediction model. They found that the dust layer extends up to 8–10 km in the warm sector of the cyclone over Mediterranean Sea, and this condition enables low dust concentration values. On the other hand, high values of the dust concentrations were found in the area of a cold front over Africa. Papayannis [17] emphasized the importance of the southerly air masses from the Sahara Desert on the high PM_{10} levels over Eastern Mediterranean Basin. Kaskaoutis [18], using satellite observations and ground-based measurements, presented Saharan dust outbreaks affecting Greece. It was found that a thick dust layer transported from Libya dramatically increased the PM_{10} concentrations (reaching up to 200 $\mu g \cdot m^{-3}$) over Athens on 17 April 2005.

In Turkey, Kubilay [5] first pointed out the origins of the dust storms affecting Erdemli, a rural site located on the coast of the EM. They presented that the region is influenced by strong dust storms originating from the central Sahara in spring, the eastern Sahara in summer, and the Middle East/Arabian Peninsula in autumn. Griffin [19] studied the relationship between Saharan sourced dust days and microorganisms over the Turkish Mediterranean coastline. They found that a statistically significant correlation during the spring months was observed between an increase in the prevalence of microorganisms recovered from atmospheric samples on dust days. Later, Koçak [20] analyzed the contributions of natural sources to high PM_{10} events for the same area. They explained that mineral dust which is transported from North Africa causes highest levels of PM_{10} during the transition period (March, April and May). Kabatas [21] investigated the possible effect of Saharan dust on high concentration levels of PM_{10} over Turkey. For this purpose, they firstly applied RAQMS (Real-Time Air Quality Modeling System) model to the intense dust storm event on April 2008 and then, they compared simulated results with the measured ones at 118-air quality stations distributed throughout the country. According to their results, RAQMS model outputs and in situ PM_{10} observation time series show similar patterns with a correlation of 0.87.

Although there are several studies concerning the origin of Saharan dust and its contributions to PM_{10} levels over Turkey, the influence of atmospheric circulation on dust concentrations has not previously been studied in detail with high spatial and temporal resolution. Therefore, the goal of the current study is to contribute to a better understanding the impacts of the synoptic mechanisms on PM_{10} concentration levels and horizontal visibility conditions over Turkey during the Saharan dust outbreaks of 23–24 March 2016.

2. Data Sources

To investigate the activity of dust plumes over Turkey, hourly and daily averages of PM_{10} data belonging to the 97 air quality monitoring stations, which were provided by the Turkish Ministry of Environment and Urbanization (National Air Quality Observation Network), were used in the study for the period 23–24 March 2016 (Figure 1). For the climatological approach, seasonal mean PM_{10} variations of these air quality stations were extracted from their daily averages for the period between 2010 and 2015. To illustrate the possible spatial and temporal variations in the plume concentrations of stations and their regional distributions, Turkey was divided into the seven geographical regions, which were described by Erinç [22], as follows: The Marmara region (MR), The Aegean region (AR), The Mediterranean region (MeR), The central Anatolian region (CAR), The Black Sea region (BSR), The eastern Anatolian region (EAR) and the southeastern Anatolian region (SEAR). To represent MR, AR, MeR, CAR, BSR, EAR, and SEAR; arithmetic averages of the PM_{10} data belonging to 9, 17, 12, 22, 15,14, and 8 air quality stations, respectively, were also used in the study. The detailed explanations of the numbered 97 air quality stations (Figure 1) such as geographic coordinates and the daily average PM_{10} concentrations belonging to 23 and 24 March dust episodes are described in Table 1.

Table 1. Geographic coordinates of the 97 air quality stations and their measured daily PM_{10} values ($\mu g \cdot m^{-3}$) during dust storm days.

No.	Region	Longitude	Latitude	Station Name	23 March 2016	24 March 2016	No.	Region	Longitude	Latitude	Station Name	23 March 2016	24 March 2016
1		26.59	41.66	Edirne	65	156	**50**		34.7	38.62	Nevsehir	49	212
2		28.89	41.04	Esenler	72	321	**51**		34.01	38.37	Aksaray	45	85
3		28.95	41.01	Aksaray	54	85	**52**		34.68	37.97	Nigde	80	188
4		29.01	41.05	Besiktas	64	274	**53**		35.38	38.74	Osb	69	186
5	Marmara (MR)	29.03	40.99	Kadikoy	72	275	**54**	Central Anatolia (CAR)	35.47	38.72	Hurriyet	95	189
6		29.21	40.89	Kartal	57	259	**55**		35.52	38.72	Melikgazi	51	126
7		29.98	40.14	Bilecik	44	116	**56**		32.51	37.94	Selcuklu	52	91
8		26.41	40.14	Canakkale	46	99	**57**		32.48	37.86	Meram	33	88
9		27.89	39.63	Balikesir	68	155	**58**		33.13	37.12	Karaman	47	121
10		29.99	39.42	Kutahya	64	86	**59**		37	39.74	Sivas	86	136
11		30.54	38.75	Afyon	33	58	**60**		33.62	40.6	Cankiri	26	28
12		29.41	38.67	Usak	87	77	**61**		31.15	40.85	Duzce	111	117
13		27.4	38.62	Manisa	128	223	**62**		31.6	40.73	Bolu	30	29
14		29.09	37.78	Merkezefendi	92	136	**63**		32.36	41.62	Bartin	98	88
15		29.1	37.77	Bayramyeri	92	120	**64**		32.62	41.2	Karabuk	95	80
16		27.84	37.84	Aydin	51	141	**65**		33.76	41.37	Kastamonu	94	147
17		28.13	37.34	Yatagan	142	115	**66**		35.15	42.03	Sinop	50	211
18	Aegean (AR)	28.36	37.22	Musluhittin	85	114	**67**		36.34	41.28	Ilkadim	81	214
19		27.07	38.5	Cigli	30	85	**68**	Black Sea (BSR)	36.46	41.22	Tekkekoy	55	158
20		27.11	38.45	Karsiyaka	16	34	**69**		34.96	40.56	Corum	76	86
21		27.17	38.46	Bayrakli	42	95	**70**		37.88	40.98	Ordu	50	86
22		27.08	38.4	Guzelyali	41	106	**71**		38.36	40.91	Giresun	66	100
23		27.22	38.47	Bornova	55	111	**72**		39.48	40.46	Gumushane	87	89
24		27.14	38.43	Alsancak	25	63	**73**		40.22	40.26	Bayburt	83	99
25		27.15	38.38	Sirinyer	44	83	**74**		40.53	41.02	Rize	40	71
26		27.14	38.31	Gaziemir	52	64	**75**		41.82	41.18	Artvin	9	13

Table 1. *Cont.*

No.	Region	Longitude	Latitude	Station Name	23 March 2016	24 March 2016	No.	Region	Longitude	Latitude	Station Name	23 March 2016	24 March 2016
27		30.29	37.72	Burdur	28	54	**76**		38.34	38.35	Malatya	39	81
28		30.7	36.89	Antalya	37	103	**77**		39.21	38.67	Elazig	33	37
29		34.64	36.81	Icel	60	66	**78**		39.55	39.1	Tunceli	20	25
30		35.26	37.19	Catalan	26	33	**79**		39.5	39.74	Erzincan	109	145
31		35.34	37	Meteoroloji	48	49	**80**		40.5	38.88	Bingol	16	27
32	Mediterranean (MeR)	35.31	37	Valilik	51	59	**81**		41.51	38.75	Mus	161	203
33		35.35	36.85	Dogankent	12	15	**82**	Eastern Anatolia (EAR)	41.27	39.9	Erzurum	26	39
34		36.24	37.07	Osmaniye	52	65	**83**		42.11	38.41	Bitlis	34	42
35		36.15	36.21	Antakya	68	72	**84**		43.74	37.57	Hakkari	64	84
36		36.9	37.58	Kahramanmaras	35	61	**85**		43.37	38.51	Van	37	43
37		37.2	38.2	Elbistan	53	59	**86**		43.04	39.72	Agri	26	36
38		30.55	37.78	Isparta	61	65	**87**		44.05	39.93	Igdir	81	100
39		30.5	39.78	Eskisehir	24	47	**88**		43.1	40.61	Kars	60	60
40		32.59	39.97	Sincan	44	59	**89**		42.7	41.11	Ardahan	22	20
41		32.8	39.97	Demetevler	57	77	**90**		37.13	36.72	Kilis	49	56
42		32.86	39.97	Kecioren	61	71	**91**		37.35	37.06	Gaziantep	43	72
43	Central Anatolia (CAR)	32.88	39.94	Cebeci	70	70	**92**		38.28	37.76	Adiyaman	59	102
44		32.86	39.93	Sihhiye	64	77	**93**	Southeastern Anatolia (SEAR)	38.79	37.16	Sanliurfa	25	75
45		32.84	39.9	Dikmen	42	79	**94**		40.22	37.92	Diyarbakir	44	46
46		32.93	39.93	Kayas	109	134	**95**		40.72	37.32	Mardin	34	62
47		33.52	39.84	Kirikkale	21	44	**96**		41.13	37.9	Batman	57	65
48		34.81	39.82	Yozgat	42	76	**97**		41.94	37.93	Siirt	89	75
49		34.16	39.15	Kirsehir	30	98							

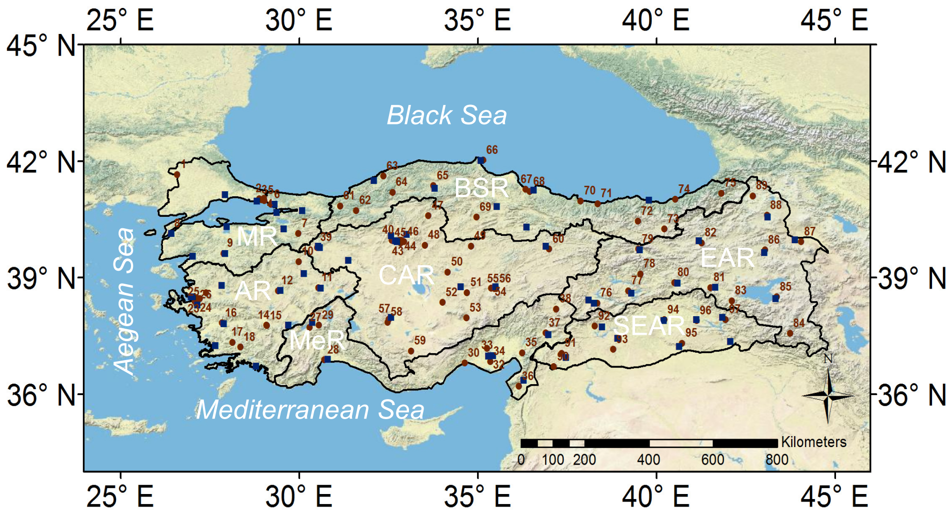

Figure 1. The distribution of PM_{10} observations at 97 air quality monitoring stations (brown points) and visibility observations (METARs, blue square) at 64 airports in Turkey. The detail explanations (i.e., geographic coordinates and daily averaged PM_{10} values of the stations during the dust storm days) of the numbers of the stations are described in Table 1. The borders of the seven geographic regions with its abbreviated names are also shown in the figure. MR: Marmara Region, AR: Aegean Region, MeR: Mediterranean Region, CAR: Central Anatolian Region, BSR: Black Sea Region, EAR: Eastern Anatolian Region, SEAR: Southeastern Anatolian Region.

The influence of these two-day extraordinary dust events on the horizontal visibility across Turkey was also investigated using the hourly observations of METAR reports at 64 airports (blue squares in Figure 1). This dataset was taken from Turkish State Meteorological Service (TSMS).

To determine the surface and upper levels of the atmospheric circulation, six- hourly values of NCEP/NCAR Reanalysis data [23] between 5° W–55° E and 30° N–60° N were applied on the extreme dust episodes. In this study, the inverse distance weighting methodology was applied for mapping METAR observations and total cloud cover data.

In order to characterize qualitatively the dust activity over Sahara and Turkey, satellite observations (Cloud-Aerosol Lidar and Infrared Pathfinder Satellite Observation (CALIPSO, provided by ICARE Data and Services Center, available at http://www.icare.univ-lille1.fr/calipso) and Meteosat Second Generation (MSG) Spinning Enhanced Visible and Infrared Imager (SEVIRI)) at high spatiotemporal resolution were used. Information about the vertical structure of the dust episode and vertical behaviors of the atmospheric conditions is provided from attenuated backscatter profiles at 532 nm retrieved from the spaceborne Cloud-Aerosol Lidar with Orthogonal Polarization (CALIOP) on board the CALIPSO together with its 60 m and 12 km vertical and horizontal resolutions, respectively. From the literature, numerous studies investigated the vertical structure of the Saharan dust outbreaks by using CALIPSO observations for Mediterranean Basin (e.g., [24–26]) and for Turkey [21]. In this study, CALIPSO observations for 23 March. and two radiosonde observations (Izmir and Kartal), which were located in western Turkey, at 00:00 UTC of March 24 were used in the analysis (The data can be accessed online at http://weather.uwyo.edu/upperair/sounding.html).

The horizontal distribution of dust was described considering the combination of three infrared channels, namely channel 10 (12 μm), channel 9 (10.8 μm), and channel 7 (8.7 μm). MSG-SEVIRI is located geostationary at 0° W over the equator and provides 15 min temporal resolution images. False-color images are created using an algorithm developed by EUMETSAT, which colors the difference between the 12.0 and 10.8 μm channels as red, the difference between the 10.8 and 8.7 μm channels as green and the 10.8 μm channel as blue (e.g., [27]). From this RGB combination, dust appears pink or magenta.

3. Results and Discussion

3.1. Seasonal Averages of PM_{10} Concentrations over Turkey

Before analyzing the extreme PM_{10} concentration levels over Turkey on March 2016, long-term seasonal averages of the 97 stations were extracted from the daily averages for the period from 2010 to 2015. Arithmetic averages of the PM_{10} concentrations related to these 97 stations indicate that highest seasonal average PM_{10} concentrations are shown in winter, fall, spring, and summer seasons over Turkey with the average values of 78, 65, 54, and 49 $\mu g \cdot m^{-3}$, respectively.

In winter, while highest mean PM_{10} values occur in the southeastern parts of the Anatolian Peninsula (i.e., SEAR: 96 $\mu g \cdot m^{-3}$), MR has the lowest concentration levels (61 $\mu g \cdot m^{-3}$ in Figure 2a). The other regions present their averaged PM_{10} concentrations within these two limits (i.e., EAR: 84 $\mu g \cdot m^{-3}$, AR: 83 $\mu g \cdot m^{-3}$, MeAR: 82 $\mu g \cdot m^{-3}$, and CAR: 75 $\mu g \cdot m^{-3}$). As shown in Figure 2a, while all of the stations in SEAR exceed 50 $\mu g \cdot m^{-3}$ on average, four of them exhibit above 100 $\mu g \cdot m^{-3}$. Moreover, 70% of the winter days exceed EU (European Union) daily limits in this region (not shown). In EAR, whereas two stations (i.e., Bingol and Tunceli) have below 50 $\mu g \cdot m^{-3}$, average PM_{10} concentration reached to 185 $\mu g \cdot m^{-3}$ in Igdir and is shown as the most polluted city over Turkey. Practically, 55% of the winter days exceed the daily EU threshold value in this region. In the Aegean region (AR), 30% of all stations that were close to the seaside showed high PM_{10} values (above 100 $\mu g \cdot m^{-3}$). As stated by Koçak [20] this condition can be explained by the transportation of sea spray.

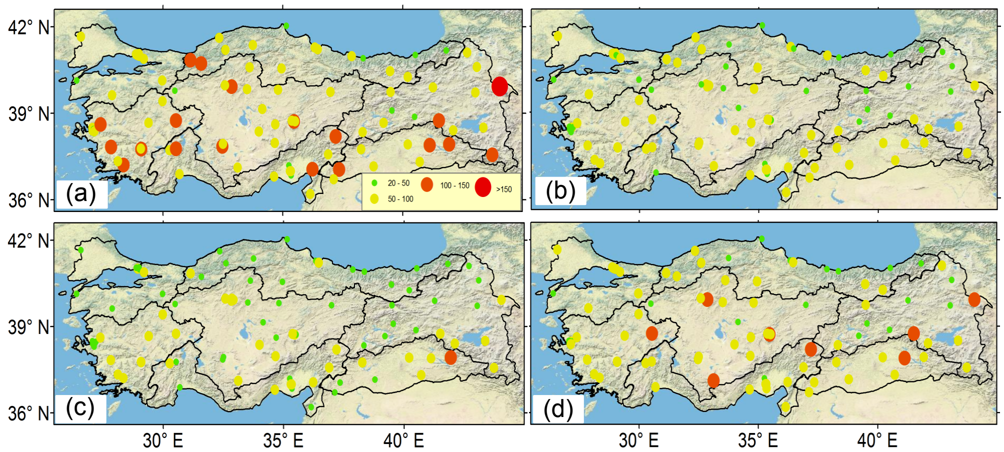

Figure 2. The long-term (2010–2015) mean of the seasonal PM_{10} concentrations ($\mu g \cdot m^{-3}$) related to 97 air quality stations. (**a**) Winter, (**b**) Spring, (**c**) Summer, and (**d**) Fall seasons, respectively.

In the transition period (spring), many Saharan dust outbreaks are transported to the EM basin and have a significant role for the excessive daily PM_{10} concentrations over Turkey. The two highest levels of PM_{10} are shown in the regions of SEAR and AR with the values of 68 and 56 $\mu g \cdot m^{-3}$, respectively. This condition can be explained by the positions of the Sharav cyclones, and thus; southerly components of the flows (i.e., SE, S, and SW) transport intense dust particles without any obstacle such as mountains. When compared with AR, geographical proximity to the source region and abundant dust particles in flat areas of the Levant basin facilitated the transportation of denser, dusty particles to SEAR. It is also known that the Tigris-Euphrates alluvial plain has been recognized as the main dust source in the Middle East [28]. Due to transferring of these intense dust particles by suitable synoptic systems, average PM_{10} values of all stations show high particulate matter concentrations (between 50 and 100 $\mu g \cdot m^{-3}$) in this basin (Figure 2b). On the other hand, while the dust particles pass over the Aegean Sea they take up moisture resulting in precipitation over the AR during spring days, therefore removing the PM via wet deposition, resulting in lower PM_{10}. As a result, average PM_{10} levels at about half of the stations were below 50 $\mu g \cdot m^{-3}$. In regard to MeR, the barrier effect of the

Taurus Mountains, a great chain running parallel to the Mediterranean coast, attenuates penetrations of Saharan dust particles to the inner parts, and thus, dust minerals are transferred only to the eastern portions of the region (Figure 2b).

Figure 2c presents 57% of all stations' average PM_{10} summer data that are below 50 $\mu g \cdot m^{-3}$ for the area over Turkey (Figure 2c). The three highest PM_{10} concentrations are observed in the SEAR, MeR, and AR basins with 65, 52, and 50 $\mu g \cdot m^{-3}$ averages, respectively. Also, highest summer mean PM_{10} level is measured in Siirt province with 103 $\mu g m^{-3}$ (Figure 2c). In fall, average PM_{10} data of eight air quality stations over the whole territory exceed 100 $\mu g \cdot m^{-3}$ with inhomogeneous spatial distribution (Figure 2d)

3.2. Spatio-Temporal Variations of Extreme Dust Episodes on 23–24 March 2016

In this section, spatial and temporal variations of the PM_{10} concentrations of air quality stations were evaluated for every two dust storm days.

The data collected for 23 March 2016 show that almost 45% of all available stations' daily PM_{10} concentrations exceeded the long-term spring mean (Figure 3a). In comparison with the daily limit threshold value, 54% of the stations exceed 50 $\mu g m^{-3}$ daily average and 6% of them display over 100 $\mu g \cdot m^{-3}$ (Table 1). In regional perspective, 80%, 67%, and 47% of the stations in the BSR, MR, and AR regions, respectively, exceed their long-term spring mean PM_{10} levels. On the other hand, daily PM_{10} data at most stations over the SEAR, EAR, and the eastern parts of the MeR exhibit below-normal values. For the CAR, mostly the inner parts of the region indicate low daily PM_{10} concentrations. In addition, the positive or negative anomaly magnitudes of the particulate matter (PM) concentrations ranged from 0 to 50 $\mu g \cdot m^{-3}$ at many of the air quality stations.

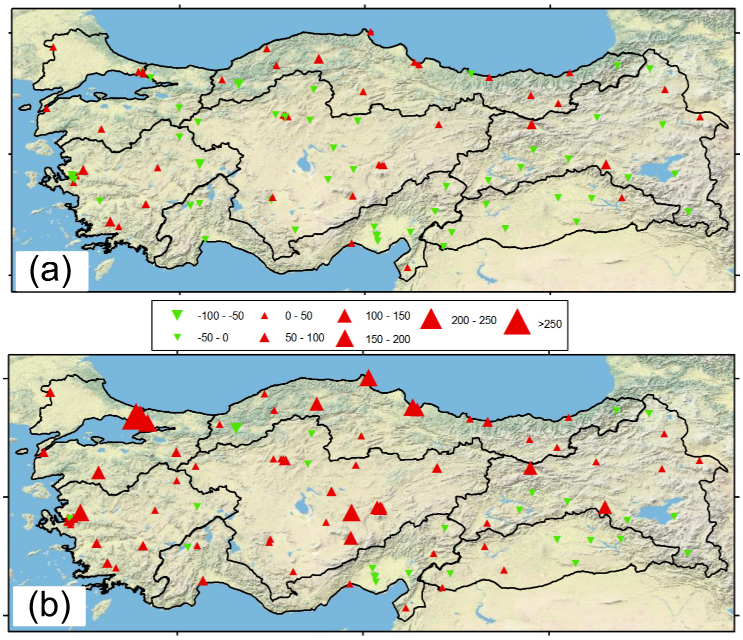

Figure 3. Anomaly values of the (**a**) March 23, 2016 and (**b**) March 24, 2016 daily PM_{10} observations ($\mu g \cdot m^{-3}$) of the stations when compared with its long-term spring mean PM_{10} values.

On 24 March 2016, the higher daily PM_{10} values were recorded at many stations of the country (Table 1 and Figure 3b). In this day, 74% of all stations show above-normal daily PM_{10} concentrations. In the regional perspective, all stations located in MR present higher daily PM_{10} anomalies, and followed by CAR (90%), AR (88%), and BSR (87%) regions, respectively. When compared with measurements from the previous day, daily PM_{10} values for certain stations turned from negative to positive anomalies over MR, AR and BSR; maximum positive variation was observed in the central part of the Anatolian Peninsula. It has also been shown that only the limited regions (i.e., SEAR and eastern portions of the MeR) illustrate the below-normal daily PM_{10} values. However, although all the stations in the SEAR have negative daily PM_{10} anomalies, all of them also exceed the EU daily PM_{10} threshold level (Table 1). In addition, most of the stations in Istanbul, (NW Turkey, most populated city in Turkey), show four times higher daily PM_{10} concentrations when compared with the long-term climatological spring means (i.e., stations numbered as 4, 5, and 6 in Table 1 and Figure 1).

To determine the starting, ending, and peak times for PM_{10} concentration levels, we analyzed the temporal behavior of the PM_{10} values for each region and the selected air quality stations (Figure 4). As shown in Figure 4a, Aegean Region reached to peak value with 104 $\mu g \cdot m^{-3}$ at 12 LT (Local Time: UTC + 2-hours) of the 23 March, and followed by decreasing trend to the 18 LT, and started to increase thereafter. The other six regions show increasing trend between 12 and 20 LT and started to decrease except Marmara Region. The increasing trend of the PM_{10} levels over Marmara continued in the first hours of the next day (Figure 4b) and reached to the maximum level at 03 LT with 413 $\mu g \cdot m^{-3}$. After 06 LT, rapid decreasing trend of the PM_{10} concentrations concluded with 24 $\mu g \cdot m^{-3}$ at the end of the day. The continued transportation of dust particles resulted with increased PM_{10} levels observed during the morning. Thereafter, PM_{10} levels started to decrease in AR. According to the results, MR is shown as the most influenced region of the country from this extraordinary event. From this point of view, it was shown that Istanbul and its surroundings have the highest PM_{10} levels, which have not measured before. Therefore, the temporal behavior of the four urban settlements of Istanbul was evaluated between 23 and 24 March, 2016. As it can be shown from Figure 4c that three urban stations (i.e., Esenler, Kartal, and Kadikoy) indicated similar increasing or decreasing tendencies in the selected time. While Esenler and Kartal air quality stations have maximum PM_{10} values at 18 LT with 139, 126 $\mu g \cdot m^{-3}$, respectively, Kadikoy area reached to its peak value at 19 LT with 153 $\mu g \cdot m^{-3}$. At the first hours of the next day (Figure 4d), highest concentration level of PM_{10} over Esenler, Kartal, Kadikoy and Besiktas were recorded with 636, 574, 564, 555 $\mu g \cdot m^{-3}$, respectively.

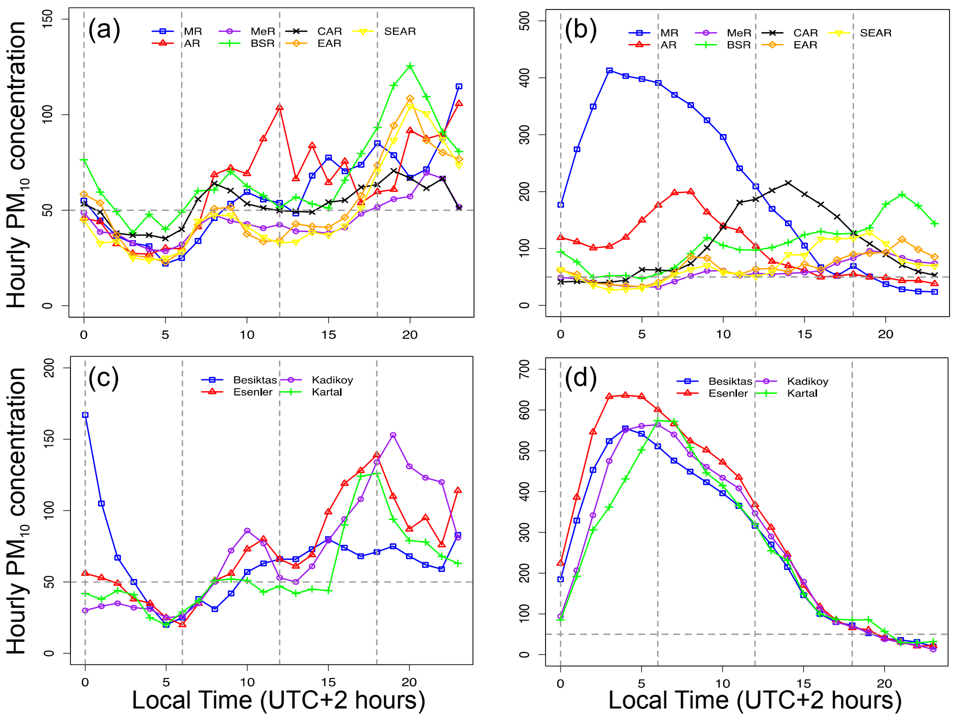

Figure 4. (**a**) Temporal behavior of the hourly PM_{10} values ($\mu g \cdot m^{-3}$) of the seven geographical regions of Turkey for 23 March, 2016. (**b**) same as (**a**) but for 24 March, 2016. (**c**) same as (**a**), and (**d**) same as (**b**) but denote the four urban settlements of Istanbul.

3.3. Association between Visibility and PM_{10} Concentrations

It is well known that there is a negative relation between visibility and atmospheric PMs. In this section, it was analyzed the influence of dust events on horizontal visibility conditions over Turkey was analyzed. For this reason, hourly observations at 64 METAR stations were used for the period of 23–24 March 2016. As a consequence of the examining horizontal visibility conditions related to the PM_{10} concentration, low visibility conditions were found between 06:00 UTC and 12:00 UTC of the 24 March 2016. The results are coherent with the previous studies that show that midday visibility is less likely to be influenced by the diurnal variation in humidity (e.g., [29]). Herewith, we used 06:00, 09:00 and 12:00 UTC METAR observations in order to investigate the spatial distribution of the low visibility over Turkey (Figure 5). At 06:00 UTC on 24 March, horizontal visibility less than 9 km is shown over the whole Marmara and western parts of the Aegean regions. In Marmara, the north areas show the lowest visibility conditions (between 3 and 4 km) over the airports owing to high particle concentrations (Figure 5a). Three hours later (09:00 UTC), while horizontal visibility started to increase between 8 and 9 km in AR, north of MR region still shows low visibility conditions (Figure 5b). At midday, although most parts of the country have clear sky conditions, the impacts of suspended particles on visibility are substantial in the limited areas of the north Marmara (between 6 and 9 km) and southern Aegean (Figure 5c). After 12:00 UTC, all stations in Turkey have high visibility conditions (not shown). According to all these results, only western parts of the country (i.e., MAR and AR) showed low visibility conditions owing to the atmospheric particulates and these conclusions are coherent with high PM_{10} concentrations (Figure 3b). However, we cannot see the inverse relation between high PM_{10} values and horizontal visibility over the BSR and CAR regions. This condition can be explained by different physical and chemical reactions of the particulate matters with ambient air conditions (e.g., different local temperature, humidity or wind profile).

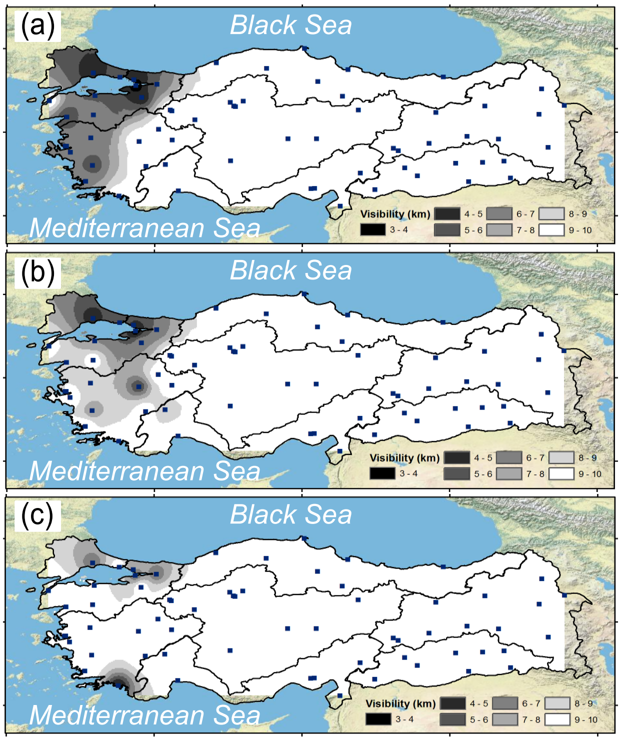

Figure 5. (**a**) Spatial distribution of the horizontal visibility conditions of the METAR observations belonging to 64 airports at 06:00 UTC of 24 March. (**b**) Same as (**a**) but for 09:00 UTC. (**c**) same as (**a**) but for 12:00 UTC.

3.4. A Review of the Synoptic Pattern of 23–24 March 2016

In this section, synoptic conditions that trigger the transportation of the pollutants over Turkey were analyzed in detail. Before the extraordinary event in Turkey, the Sharav cyclone over the lee of the Moroccan Atlas mountains, and high-pressure center (HPC) over Egypt settled in the area over latitude of 30–35° N. As a result, dense dust particles were transported to the central Mediterranean basin on 22 March, 2016 (not shown). It was shown 24-hours later that Sharav cyclone developed (985-hpa in the core) and moved to Italy in the direction of NE. Simultaneously, surface high pressure moved more east and settled over Levant basin (Figure 6a). On the other hand, cut off-surface low over the western Russia expanded towards to Black Sea. Ultimately, the mobilization of Saharan dust plumes turned to the eastern Mediterranean basin. In terms of the low level of the atmosphere at that time (Figure 6b), the positions of the low- and high-pressure centers were similar to those of the centers of the surface, and most regions of Turkey were influenced by strong southwesterly wind flows (over 30 m·s^{-1}). While positions of the surface- and 850-hPa- low centers remain almost stationary at 12:00 UTC, expanding of surface- and low-level highs above southeastern Turkey leaded to more strong southerly winds (i.e., high pressure gradient situation) over the western parts of the country (Figure 6c,d). Hence, rapid increment in aerosol load over the Aegean region is more distinct than the other regions of Turkey at the midday of the 23 March (Figure 4a). Differently from the other regions, the anticyclonic conditions over SEAR prevented transferring of particles, which originated from Sahara, to this region (Figure 3a).

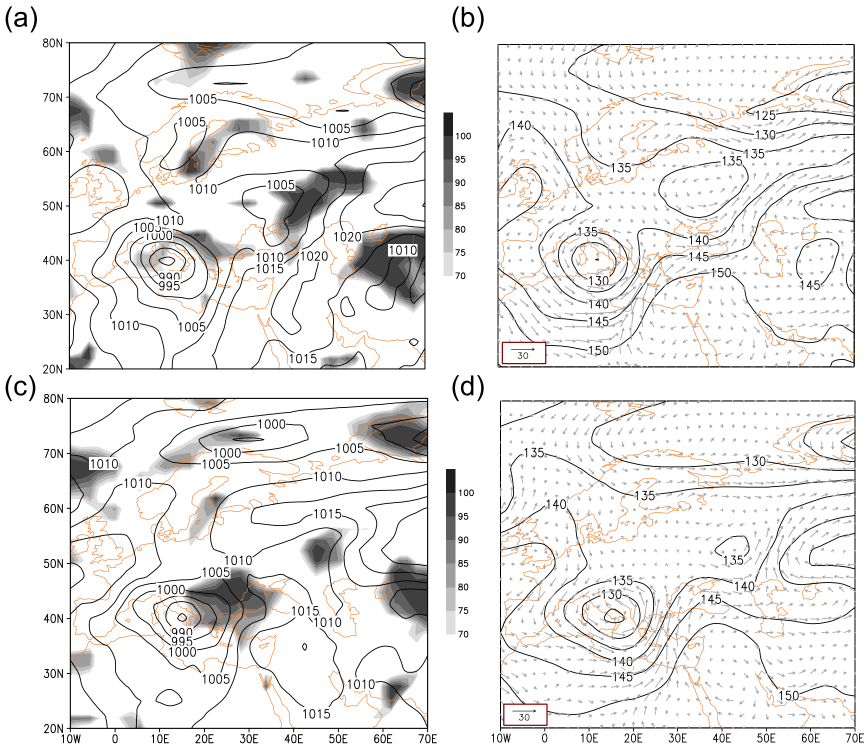

Figure 6. The evolution of the first dust storm event over Turkey at 00:00 UTC 23 March 2016. (**a**) sea level pressures (solid lines, every 5-hPa), and total cloud cover (shaded, %) at surface. (**b**) Height (solid lines, dam) and winds (m·s^{-1}) at 850-hPa. (**c**) same as (**a**), and (**d**) same as (**b**) but for 12:00 UTC of the 23 March.

The temporal movements of dust layers can be analyzed using satellite images. Therefore, we extracted the RGB product of the three SEVIRI infrared channels for 12:00 and 18:00 UTC of 23 March. The dust appears pink and is concentrated into several plumes in Figure 7. As seen in Figure 7a, a thick dust layer from Libya is transported to the Aegean coasts of Greece, and relatively high PM_{10}

values were observed in the AR regions of Turkey. At 18:00 UTC, ongoing movement of the particles to east longitudes resulted with highest PM_{10} values over the large areas of the country (Figure 7b).

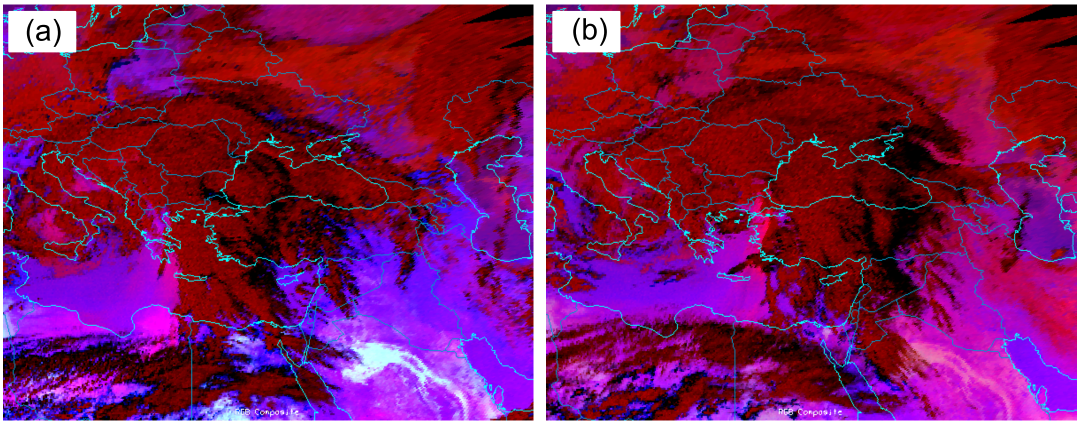

Figure 7. Dust product for (**a**) 12:00 UTC and (**b**) 18:00 UTC on 23 March 2016, derived from three infrared channels of the SEVIRI imager on Meteosat-10, with center wavelengths at 12.0, 10.8, and 8.7 μm. This false-color image was created using an algorithm from EUMETSAT, which colors red the difference between the 12.0 and 10.8 μm channels, green the difference between the 10.8 and 8.7 μm channels and blue the 10.8 μm channel. Dust appears pink or magenta, water vapor dark blue, thick high-level clouds red-brown, thin high-level clouds almost black and surface features pale blue or purple.

On March 24 at 00:00 UTC, only the zonal movement of surface- and 850-hpa low- centers from 15° E to 20° E (from Italy to Balkan Peninsula) resulted with penetration of strong south and southwesterly winds over the most regions of the Anatolian Peninsula (Figure 8a,b). That day, 74% of air quality stations showed above-normal PM_{10} concentrations (Figure 3b). In regional perspective, coarse PM increment was more remarkable in MR than the other parts of the country and over 600 $\mu g \cdot m^{-3}$ concentration values were measured over the urban settlements of Istanbul (e.g., Esenler) in these hours (Figure 4b,d). South and southwesterly winds turned into the westerly winds owing to the rapid movement of this cyclone to more northeast (over Black Sea) at 12-hours later (Figure 8c,d) and thus; PM_{10} concentration levels started to decrease in the whole county from the highest points (Figure 4b).

It is well known from the previous studies that, omega winds in the context of the synoptic perspective show the upward and downward movements of the dust particles (e.g., [14,30,31]). From this viewpoint, the omega winds at 1000-hPa synoptic map were extracted for 00:00 UTC of March 24, available time for the observed dense particles over Turkey. As shown in Figure 9, sink regions (positive values) owing to the strong downward movements of the air are shown over the Black Sea and thus; transported dust can easily be subside in this region of the country.

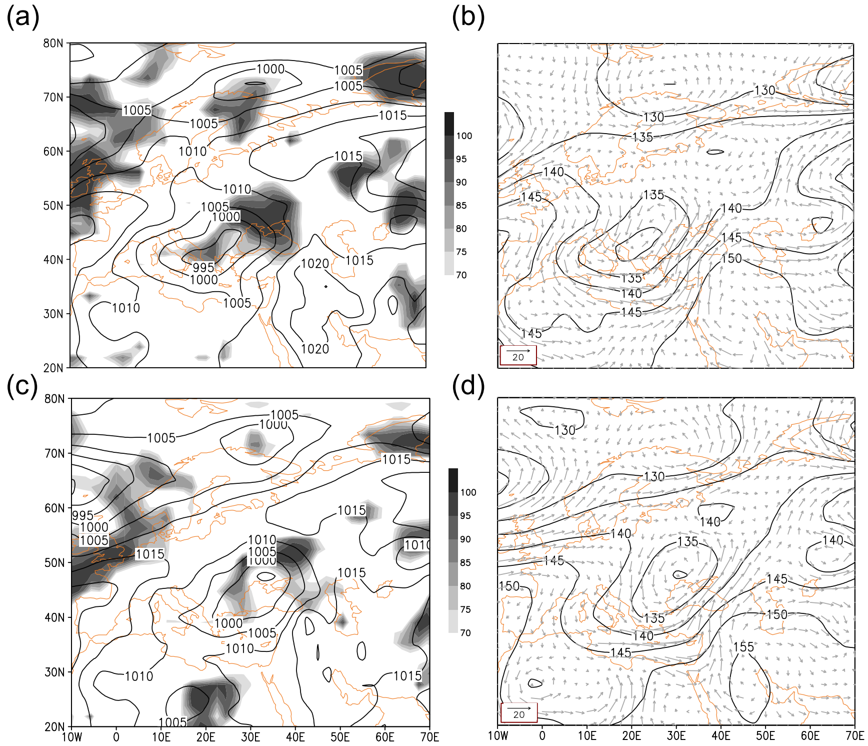

Figure 8. The evolution of the second dust storm event over Turkey at 00:00 UTC 24 March 2016. (**a**) sea level pressures (solid lines, every 5-hPa), and total cloud cover (shaded, %) at surface. (**b**) Height (solid lines, dam) and winds ($m \cdot s^{-1}$) at 850-hPa. (**c**) same as (**a**) and (**d**) same as (**b**) but for 12:00 UTC of the 24 March.

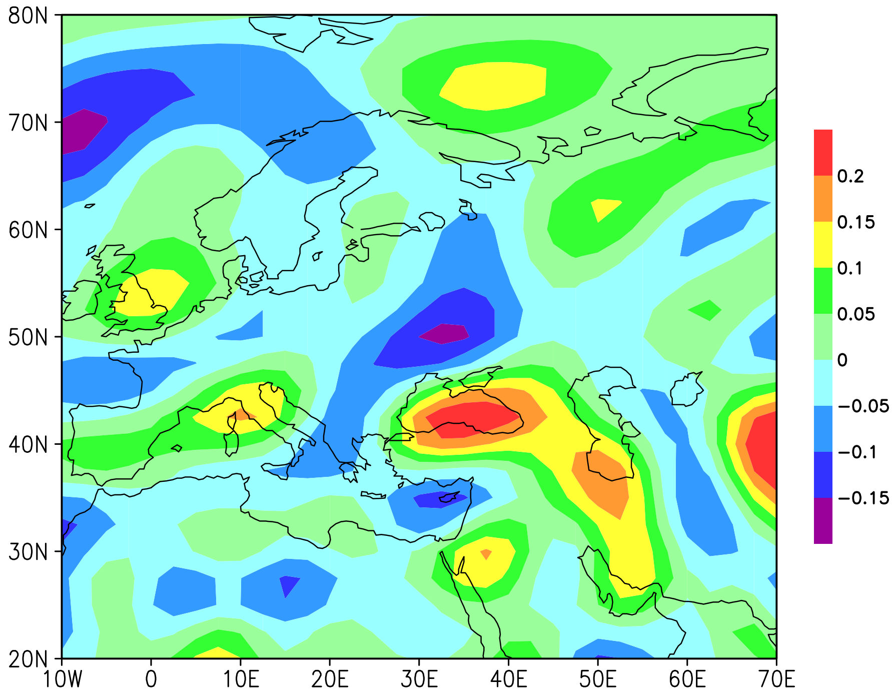

Figure 9. Omega map ($Pa \cdot s^{-1}$) at 1000-hPa for 24 March 00:00 UTC. Red-to-yellow area corresponds to a sink area, while negative values show upward movement of air.

3.5. Vertical Profiles of Saharan Dust

Figure 10a shows the ground track of the CALIPSO orbit and the altitude orbit cross-section measurement of ß532 during the southward descent of the night flight of the CALIPSO on 23 March 2016. It was chosen this time and day because the CALIPSO profiles for the other times and days are unavailable due to its transport route (flies only once every 16 days over a defined site) and unfavorable weather conditions such as presence of thick clouds. The attenuated backscatter quick-looks derived from CALIOP on board CALIPSO satellite indicate that aerosol-loaded plumes were distributed from the near-ground surface to an altitude of 8 km between 24.5° N and 26.5° N. Most of the aerosol load is shown between 2 and 4 km in these source regions. To illustrate the vertical behavior of the suspended dust particles during transportation, we analyzed the atmospheric sounding observations of Izmir (WMO number 17220, as a representative Aegean station, 38.43° N, 27.16° E) and Kartal (WMO number 17064, as a representative station of Marmara, 40.90° N, 29.15° E) for the 00:00 UTC of March 24. From Figure 10b, a thin inversion layer at 700-hPa is shown in Izmir. This level is important for Saharan originated dust particles, which are transported to the eastern Mediterranean and generally enriched with important aerosol loads [17]. When we compared with the previous day's radiosonde profile (23 March 00:00 UTC, not shown), the atmosphere is fully saturated from ground to this level. Based on METARs reports numerous convective precipitation events between 00:00 UTC and 12:00 UTC were observed at stations located in AR (not shown). In conclusion, both thin inversion layer at mid-level of the atmosphere and removal mechanism of the precipitation prevented us showing highest PM concentration levels in the AR. For Marmara, thick inversion level near the ground surface on the previous day shows parallelism on 24 March and restricts the escape of the dust particles to upper levels. In addition to this, dry atmospheric conditions enable us to observe the highest PM_{10} observations at this date, which had never been recorded (Figure 10c).

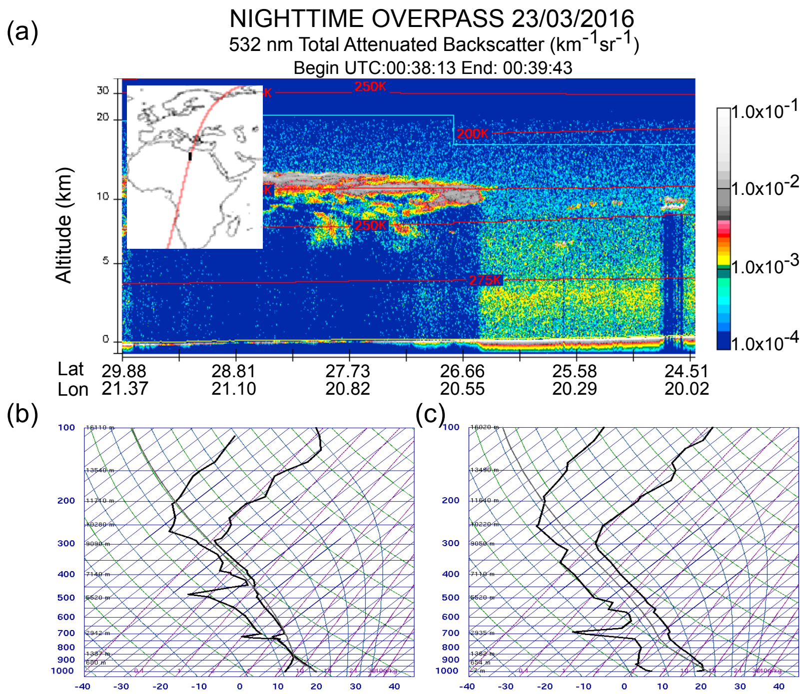

Figure 10. (**a**) Attenuated backscatter quicklook derived from CALIOP (CALIPSO satellite on 23 March 2016 at night during the over passes over the dust source region. (**b**) Skew T-logp diagram of Izmir (western station, WMO number: 17220) at 00:00 UTC of 24 March, 2016. The solid thick lines represent temperature and dewpoint observations. Temperature in °C and pressure levels in hPa. (**c**) same as (**b**) but for Kartal (northern station, WMO number: 17064)

4. Summary and Conclusions

It is well known that the Saharan dust outbreaks are frequently transported to western Turkey in spring months. In one of the latest Saharan dust episodes, high particulate matter concentrations were observed in the larger area of the Anatolian Peninsula between 23 and 24 March of 2016. Therefore, the spread of dust over Turkey and its effect on horizontal visibility have been investigated using PM_{10} observations from 97 air quality stations, and METAR observations from 64 airports. These two-day synoptic considerations of high dust events were analyzed using synoptic charts, and satellite images were also used in the analyses.

A severe dust storm event occurred during the late quarter of March 2016. On 23 March 2016, Sharav cyclone developed and moved from its origin to Italy in NE direction. On the other side, surface high pressure simultaneously was settled over the Levant basin. Maintaining similar positions of the low (high) centers at 850-hPa with its surface pressure centers enabled us to observe strong southwesterly wind flows over Turkey. As a consequence, 45% of all stations exceeded their long-term means (54% showed daily limit values above those proposed by the EU). In a regional approach, northern and western parts of the country (i.e., Black Sea, Marmara, and Aegean regions) are most influenced from these strong dust plumes. Anticyclonic conditions over southeastern Anatolia prevented loading of the dust particles to this region.

During the beginning of the 24 March 2016, zonal shifting of the low (pressure) centers from Italy to the Balkan Peninsula and quasi-stationary conditions of the high (pressure) centers facilitate rapid and dense transport of a thick Saharan dust layer (between 2 and 4 km) to Anatolian Peninsula under favor of strong south-southwestern winds. As a consequence, 74% of the 97 air quality stations showed above-normal PM_{10} concentrations. In a regional perspective, 100%, 90%, 88%, and 87% of the stations in Marmara (NW Turkey), central Anatolia, western (Aegean) and northern (Black Sea) portions of Turkey, respectively, exhibited above-normal daily PM_{10} values. For northern Turkey (BSR), subsidence at low-levels plays a significant role in observing above-normal PM_{10} concentrations. While occurring of some convective precipitation events over Aegean Region and thin inversion level at mid-level of the atmosphere (700-hPa) prevent excessive increase of PM_{10} levels in this region. When particles moved more north under the same synoptic conditions, a thick inversion layer near the ground surface restricted the escape of the suspended air particles from Marmara. In conclusion, the highest PM_{10} levels are shown in MR (on average, 413 $\mu g \cdot m^{-3}$ at 03 LT); peak values reached over 550 $\mu g \cdot m^{-3}$ in the four urban settlements of Istanbul (Esenler, Kartal, Kadikoy, and Besiktas) at 03 LT. When examined on a diurnal basis, the PM_{10} levels of these four stations were almost four times higher than their long-term spring means, and almost 1.5-fold higher than the previous spring's peak daily PM_{10} values. It was also shown that visibility decreased to 3–4 km in the north of Marmara, especially in the metropolitan city of Istanbul. Thus, there were significant negative effects of Saharan dust outbreaks on aviation activities. Combination of large dust storms coupled with cyclonic activities should definitely be a point of consideration in forecasting low visibility and above-normal PM_{10} values over the particular or whole terrain of Turkey.

Conflicts of Interest: The author declares no conflict of interest.

References

1. Goudie, A.S.; Middleton, N.J. Saharan dust storms: Nature and consequences. *Earth-Sci. Rev.* **2001**, *56*, 179–204. [CrossRef]
2. Chiapello, I.; Bergametti, G.; Gomes, L.; Chatenet, B.; Dulac, F.; Pimenta, J.; Santos Suares, E. An Additional Low Layer Transport of Sahelian and Saharan Dust over the North-Eastern Tropical Atlantic. *Geophys. Res. Lett.* **1995**, *22*, 3191–3194. [CrossRef]
3. Kellogg, C.A.; Griffin, D.W.; Garrison, V.H.; Peak, K.K.; Royall, N.; Smith, R.R.; Shinn, E.A. Characterization of aerosolized bacteria and fungi from desert events in Mali, West Africa. *Aerobiologia* **2004**, *20*, 99–110. [CrossRef]

4. Perez, L.; Tobias, A.; Querol, X.; Künzli, N.; Pey, J.; Alastuey, A.; Viana, M.; Valero, N.; Gonzales-Cabre, M.; Sunyer, J. Coarse particles from Saharan dust and daily mortality. *Epidemiology* **2008**, *19*, 800–807. [CrossRef] [PubMed]
5. Kubilay, N.; Cokacar, T.; Oguz, T. Optical properties of mineral dust outbreaks over the northeastern Mediterranean. *J. Geophys. Res.* **2003**, *108*, 4666. [CrossRef]
6. Akpinar-Elci, M.; Martin, F.E.; Behr, J.G.; Diaz, R. Saharan dust, climate variability, and asthma in Grenada, the Caribbean. *Int. J. Biometeorol.* **2015**, *59*, 1667–1671. [CrossRef] [PubMed]
7. Jimenez, E.; Linares, C.; Martinez, D.J. Role of Saharan dust in the relationship between particulate matter and short-term daily mortality among the elderly in Madrip (Spain). *Sci. Total Environ.* **2010**, *408*, 5729–5736. [CrossRef] [PubMed]
8. Mate, T.; Guaita, R.; Pichiule, M.; Linares, C.; Diaz, J. Short-term effect of fine particulate matter ($PM_{2.5}$) on daily mortality due to diseases of the circulatory system in Madrid (Spain). *Sci. Total Environ.* **2010**, *408*, 5750–5757. [CrossRef] [PubMed]
9. Middleton, N.; Yiallouros, P.; Kleanthous, S.; Kolokotroni, O.; Schwartz, J.; Dockery, D.W.; Demokritou, P.; Koutrakis, P. A 10-year time-series analysis of respiratory and cardiovascular morbidity in Nicosia, Cyprus: The effect of short-term changes in air pollution and dust storms. *Environ. Health* **2008**, *7*, 39. [CrossRef] [PubMed]
10. Samoli, E.; Kougea, E.; Kassomenos, P.; Analitis, A.; Katsouyanni, K. Does the presence of desert dust modify the effect of PM_{10} on mortality in Athens, Greece? *Sci. Total Environ.* **2011**, *409*, 2049–2054. [CrossRef] [PubMed]
11. Zauli Sajani, S.; Miglio, R.; Bonasoni, P.; Cristofanelli, P.; Marinoni, A.; Sartini, C.; Goldoni, C.A.; de Girolamo, G.; Lauriola, P. Saharan dust and daily mortality in Emilia-Romagna (Italy). *Occup. Environ. Med.* **2011**, *68*, 446–451. [CrossRef] [PubMed]
12. Alpert, P.; Kishcha, P.; Shtivelman, A.; Krichak, S.O.; Joseph, J.H. Vertical distribution of Saharan dust based on 2.5-year model predictions. *Atmos. Res.* **2004**, *70*, 109–130. [CrossRef]
13. Bangert, M.; Nenes, A.; Vogel, B.; Vogel, H.; Barahona, D.; Karydis, V.A.; Kumar, P.; Kottmeier, C.; Blahak, U. Saharan dust event impacts on cloud formation and radiation over Western Europe. *Atmos. Chem. Phys.* **2012**, *12*, 4045–4063. [CrossRef]
14. Cabello, M.; Orza, J.A.G.; Barrero, M.A.; Gordo, E.; Berasaluce, A.; Canton, L.; Duenas, C.; Fernandes, M.C.; Perez, M. Spatial and temporal variation of the impact of an extreme Saharan dust event. *J. Geophys. Res.* **2012**, *117*, D11204. [CrossRef]
15. Moulin, C.; Lambert, C.E.; Dayan, U.; Masson, V.; Ramonet, M.; Bousquet, P.; Legrand, M.; Blakanski, Y.J.; Guella, W.; Marticorena, B.; Bergametti, G.; Dulac, F. Satellite climatology of African dust transport in the Mediterranean atmosphere. *J. Geophys. Res.* **1998**, *103*, 13137–13144. [CrossRef]
16. Tsidulko, M.; Krichak, S.O.; Alpert, P.; Kakaliagou, O.; Kallos, G.; Papadopoulos, A. Numerical study of a very intensive eastern Mediterranean dust storm, 13–16 March 1998. *J. Geophys. Res.* **2002**, *107*, 4581. [CrossRef]
17. Papayannis, A.; Balis, D.; Amiridis, V.; Chourdakis, G.; Tsaknakis, G.; Zerefos, C.; Castanho, A.D.A.; Nickovic, S.; Kazadzis, S.; Grabowski, J. Measurements of Saharan dust aerosols over the Eastern Mediterranean using elastic backscatter-Raman lidar, spectrophotometric and satellite observations in the frame of the EARLINET project. *Atmos. Chem. Phys.* **2005**, *5*, 2065–2079. [CrossRef]
18. Kaskaoutis, D.G.; Kambezidis, H.D.; Nastos, P.T.; Kosmopoulos, P.G. Study on an intense dust storm over Greece. *Atmos. Environ.* **2008**, *42*, 6884–6896. [CrossRef]
19. Griffin, D.W.; Kubilay, N.; Koçak, M.; Gray, M.A.; Borden, T.C.; Shinn, E.A. Airborne desert dust and aeromicrobiology over the Turkish Mediterranean coastline. *Atmos. Environ.* **2007**, *41*, 4050–4062. [CrossRef]
20. Koçak, M.; Mihalopoulos, N.; Kubilay, N. Contributions of natural sources to high PM_{10} and $PM_{2.5}$ events in the eastern Mediterranean. *Atmos. Environ.* **2007**, *41*, 3806–3818. [CrossRef]
21. Kabatas, B.; Unal, A.; Pierce, R.B.; Kindap, T.; Pozzoli, L. The contribution of Saharan dust in PM_{10} concentration levels in Anatolian Peninsula of Turkey. *Sci. Total Environ.* **2014**, *488–489*, 413–421. [CrossRef] [PubMed]
22. Erinç, S. *Climatology and Its Methods*, 3rd ed.; Istanbul, Gür-ay Pres Inc.: Istanbul, Turkey, 1984. (in Turkish)

23. Kalnay, E.; Kanamitsu, M.; Kistler, R.; Collins, W.; Deaven, D.; Gandin, L.; Iredell, M.; Saha, S.; White, G.; Wollen, J.; et al. The NCEP/NCAR 40 year reanalysis project. *Bull. Am. Meteorol. Soc.* **1996**, *77*, 437–471. [CrossRef]
24. De la Paz, D.; Vedrenne, M.; Borge, R.; Lumbreras, J.; de Andres, J.M.; Perez, J.; Rodriguez, E.; Karanasiou, A.; Moreno, T.; Boldo, E.; Linares, C. Modelling Saharan dust transport into the Mediterranean basin with CMAQ. *Atmos. Res.* **2013**, *70*, 337–350. [CrossRef]
25. Guerrero-Rascado, J.L.; Olmo, F.J.; Aviles-Rodriguez, I.; Navas-Guzman, F.; Perez-Ramirez, D.; Lyamani, H.; Arboledas, L.A. Extreme Saharan dust event over the southern Iberian Peninsula in September 2007: Active and passive remote sensing from surface and satellite. *Atmos. Chem. Phys.* **2009**, *9*, 8453–8469. [CrossRef]
26. Mona, L.; Amodeo, A.; Pandolfi, M.; Pappalardo, G. Saharan dust intrusions in the Mediterranean area: Three years of Raman lidar measurements. *J. Geophys. Res.* **2006**, *111*, D16203. [CrossRef]
27. Schepanski, K.; Tegen, I.; Laurent, B.; Heinold, B.; Macke, A. A new Saharan dust source activation frequency map derived from MSG-SEVIRI IR-channels. *Geophys. Res. Lett.* **2007**, *34*, L18803. [CrossRef]
28. Hamidi, M.; Kavianpour, M.R.; Shao, Y. Synoptic analysis of dust storms in the Middle East. *Asia-Pac. J. Atmos. Sci.* **2013**, *49*, 279–286. [CrossRef]
29. Vajanapoom, N.; Shy, C.M.; Neas, L.M.; Loomis, D. Estimation of particulate matter from visibility in Bangkok, Thailand. *J. Expo. Sci. Environ. Epidemiol.* **2001**, *11*, 97–102. [CrossRef]
30. Ganor, E.; Stupp, A.; Osetinsky, I.; Alpert, P. Synoptic classification of lower troposphere profiles for dust days. *J. Geophys. Res.* **2010**, *115*, D11201. [CrossRef]
31. Prasad, A.K.; El-Askary, H.; Kafatos, M. Implications of high altitude desert dust transport from Western Sahara to Nile Delta during biomass burning season. *Environ. Pollut.* **2010**, *158*, 3385–3391. [CrossRef] [PubMed]